Research Square

Preprints are preliminary reports that have not undergone peer review.
They should not be considered conclusive, used to inform clinical practice,
or referenced by the media as validated information.

Strain-specific mobile antiphage defense systems restrict virulence factor-encoding temperate phages in Staphylococcus aureus

Kohei Kondo

kondo.ko@jihs.go.jp

Japan Institute for Health Security, National Institute of Infectious Diseases https://orcid.org/0009-0006-6451-2728

Shoko Kutsuno

National Institute of Infectious Diseases

Yo Sugawara

National Institute of Infectious Diseases https://orcid.org/0000-0002-9897-3905

Aa Haeruman Azam

Japan Institute for Health Security

Kotaro Kiga

Department of Drug Development, National Institute of Infectious Diseases, Japan Institute for Health Security

Kasumi Kuroki

Japan Institute for Health Security, National Institute of Infectious Diseases

Mitsuoki Kawano

Nakamura Gakuen University

Shizuo Kayama

Japan Institute for Health Security, National Institute of Infectious Diseases

Manami Tsunoi

Japan Institute for Health Security, National Institute of Infectious Diseases

Miyo Murai

Saitama Prefectural University

Kozue Kishii

Saitama Prefectural University

Makoto Ohnishi

Japan Institute for Health Security, National Institute of Infectious Diseases

Motoyuki Sugai

National Institute of Infectious Diseases https://orcid.org/0000-0001-9252-7739

Junzo Hisatsune

Japan Institute for Health Security, National Institute of Infectious Diseases

Article

Keywords:

Posted Date: September 21st, 2026

DOI: https://doi.org/10.21203/rs.3.rs-11084139/v1

License: This work is licensed under a Creative Commons Attribution 4.0 International License.
Read Full License

Additional Declarations: There is **NO** Competing Interest.

Abstract

Staphylococcus aureus acquires virulence factor (VF) genes through temperate phages; however, determinants of strain-specific permissiveness to these mobile genetic elements remain poorly understood. Here, we isolated 11 temperate phages from 254 genetically diverse *S. aureus* isolates and determined their complete genome sequences, identifying VF-encoding phages carrying exfoliative toxin A, Panton–Valentine leukocidin, and immune-evasion genes. Host-range profiling across 58 clinical isolates representing 16 sequence types revealed substantial variations in susceptibility between and within lineages. Within clonal complex 5, we identified two mobile defense systems, *stk2* and a *mad1*-like operon, which reduced the plating efficiency of multiple VF-encoding temperate phages 10^2–10^7-fold post-adsorption. Across 21,509 *Staphylococcaceae* genomes, *mad1*-like loci occurred in approximately 15% and were typically inserted adjacent to prophage integrase genes. These findings support a hierarchical model in which lineage- and strain-specific defense repertoires collectively shape permissiveness to the VF-encoding temperate phages.

Introduction

Staphylococcus aureus is a versatile gram-positive opportunistic pathogen responsible for a broad spectrum of diseases, ranging from superficial skin and soft-tissue infections to life-threatening invasive infections, as well as toxin-mediated illnesses such as staphylococcal food poisoning [1, 2]. The clinical manifestations of *S. aureus* infections are shaped by the repertoire of virulence factors (VFs) carried by individual strains [3, 4]. Among these, exfoliative toxins induce epidermal cleavage through the proteolytic degradation of desmoglein-1, leading to the characteristic skin lesions of impetigo and staphylococcal scalded skin syndrome (SSSS), particularly in infants and young children [5, 6, 7]. Panton–Valentine leukocidin (PVL) targets neutrophils and other leukocytes, contributing to soft-tissue necrosis and abscess formation, and has been associated with severe clinical manifestations, including necrotizing pneumonia [8, 9, 10, 11]. Staphylococcal enterotoxins (SEs), a family of heat-stable superantigenic exotoxins, cause staphylococcal food poisoning through the ingestion of preformed toxins, with SEA being the serotype most frequently implicated in outbreaks [2].

Many of these VFs are encoded by temperate phages or phage-related mobile genetic elements (MGEs). Exfoliative toxin A (*eta*), staphylococcal enterotoxin (*sea*), and PVL (*lukF-PV* and *lukS-PV*) are associated with distinct families of temperate phages [12]. These phages facilitate the horizontal dissemination of virulence genes and are thought to contribute to the evolution of clinically important lineages.

Despite these lineage-level associations, carriage of VF-encoding temperate phages frequently varies among strains belonging to the same sequence type (ST) or clonal complex (CC), indicating that clonal background alone does not determine host permissiveness to MGEs [13, 14]. Because the acquisition of VF-encoding MGEs is closely linked to the emergence of clinically significant clones, it is essential to identify the determinants of strain-specific permissiveness. However, the underlying mechanisms remain

incompletely defined [15, 16]. Consistent with this concept, our nationwide genomic surveillance of *S. aureus* isolates from bloodstream infections in Japan demonstrated that several clinically prevalent lineages, including ST188, ST15, ST20, ST25, and ST121, consistently harbored fewer antimicrobial resistance genes (ARGs), virulence factor genes (VFGs), and MGEs than did ST1, ST5, or ST8 [17]. Recently, we identified SadR, an RNase-mediated antiphage defense factor that restricts bacteriophage and plasmid acquisition, thereby limiting the horizontal transfer of MGEs, including Staphylococcal Cassette Chromosomal *mec* (SCC*mec*), in *S. aureus* [18]. In that study, we established lineage-specific intracellular antiphage defense as an important determinant of host permissiveness to horizontal gene transfer. However, the observed heterogeneity in phage permissiveness among strains within individual lineages suggests that additional strain-specific defense mechanisms remain to be identified.

The phage–host range can be classically explained at the level of adsorption [19, 20]. In *S. aureus*, the primary receptor is wall teichoic acid (WTA), and variation in WTA glycosylation contributes to differences in susceptibility among *S. aureus* lineages [20, 21, 22]. However, successful phage infection also depends on the intracellular events following phage DNA injection. Comparative genomic analyses using DefenseFinder and PADLOC have revealed a remarkably diverse repertoire of antiphage defense systems in *S. aureus* in addition to conserved restriction-modification (RM) systems [23, 24]. These observations suggest that intracellular defense systems provide an additional layer of protection beyond receptor-mediated adsorption. However, it remains unknown whether additional strain-specific antiphage defense systems govern the acquisition and host range of VF-encoding temperate phages among clinically important *S. aureus* lineages.

In this study, we investigated the determinants of strain-specific host permissiveness to VF-encoding temperate phages by combining phage isolation, host-range profiling, comparative genomics, and functional validation. We isolated 11 temperate phages from 254 *S. aureus* isolates of clinical, companion animal, and sewage origin, several of which encoded genes for major VFs, including exfoliative toxin A (ETA), PVL (LukF-PV/LukS-PV), and SEs. We systematically determined their host ranges using 58 strains representing 16 STs. By focusing on lineage-matched susceptible and non-susceptible strains within CC5, we identified and functionally validated two strain-specific defense determinants, *stk2* and a *mad1*-like operon, that markedly restrict infection by multiple VF-encoding temperate phages. Our findings demonstrate that strain-specific intracellular antiphage defenses shape host permissiveness to VF-encoding temperate phages and may contribute to the lineage- and strain-dependent dissemination of VF-encoding temperate phages and their associated virulence genes.

Results

Isolation and genomic characterization of 11 S. aureus temperate phages

We screened 254 *S. aureus* isolates obtained from clinical specimens, companion animals, and sewage-derived samples for mitomycin C-inducible prophages. Phage lysates were obtained from 39 isolates, and 11 phages yielded genome sequences of sufficient quality for subsequent genomic and phenotypic

analyses (Supplementary Table 1). These 11 phages originated from donor strains spanning diverse sources, STs, and VF profiles (Fig. 1A, Supplementary Table 2). Whole-genome sequencing analysis revealed that eight of the 11 phages carried at least one VFG: phiJP42, phiJP43, phiJP72, phiSewage2, and phiSewage3 encoded the ETA gene (*eta*); phiMW2 encoded the PVL genes (*lukF-PV/lukS-PV*); phiUSA300 encoded the immune-evasion cluster genes *sak* (staphylokinase), *chp* (chemotaxis inhibitory protein), and *scn* (staphylococcal complement inhibitor); and phiVDT12 encoded the staphylococcal enterotoxin A gene (*sea*) together with *sak* and *scn* (Supplementary Table 2).

To place the 11 newly isolated temperate phages within the broader diversity of *S. aureus* phages, we constructed a viral proteomic tree of these 11 phages together with 193 reference *S. aureus* phages using ViPTree. The 11 isolated phages were distributed across diverse clusters of known *S. aureus* temperate phages, with genome sizes ranging from approximately 42 to 46 kb, consistent with those of other *S. aureus* temperate phages (Fig. 1A).

Next, we compared each isolated phage genome to the closest reference phage in the ViPTree tree (light orange in Fig. 1A; all pairwise intergenomic similarities are provided in Supplementary Table 3). Among the *eta*-carrying phages, phiJP42 and phiJP43 were closely related to ΦETA2 (RefSeq accession NC_008798), a member of the genus *Dubowvirus*, sharing > 99% nucleotide identity across the aligned regions; phiSewage2 and phiSewage3 clustered with ΦETA (NC_003288) and shared 98.2% nucleotide identity; and phiJP72 was closely related to ΦETA3 (NC_008799) at > 99% nucleotide identity (Fig. 1B). phiMW2 was most closely related to phiSa2wa_st1 (NC_055045), with 92.9% intergenomic similarity, and both phages carried the *lukF-PV/lukS-PV* genes. In contrast, although phiUSA300 was induced in the PVL-positive USA300 strain, it did not encode *lukF-PV/lukS*-PV; instead, it carried the immune-evasion cluster genes, including *sak*, *chp*, and *scn*. phiUSA300 was highly similar to phage 23MRA (NC_028775), with > 99% nucleotide identity; both phages encoded *sak*, *chp*, and *scn*. The VDT-derived phage phiVDT12, which carries three VFGs (*sea*, *sak*, and *scn*), was most closely related to the SA780ruMSSAST101 phage (NC_048644, *Peeveelvirus*) with 85.6% intergenomic similarity; *sak* and *scn* were shared between the two phages, whereas *sea* was unique to phiVDT12. In contrast, phiJP49, phiSewage6, and phiJP152 did not encode known VFGs and shared < 90% intergenomic similarity with their closest reference phages (Supplementary Table 3), suggesting that they represent comparatively divergent lineages within the *S. aureus* temperate phage population.

Host range of S. aureus temperate phages varies by strain

To evaluate phage infectivity across diverse lineages, we performed host range assays using a panel of 58 clinical *S. aureus* isolates representing 16 STs, comprising 55 clinical isolates collected in Japan and the reference strains MW2, USA300, and RN4220 (Supplementary Table 4). These isolates harbored heterogeneous repertoires of MGEs, including prophages and *S. aureus* pathogenicity islands (SaPIs; Supplementary Table 4, Supplementary Fig. 1, Fig. 2). Most of the 11 phages infected strains across multiple STs. For example, the ΦETA-like phages phiSewage2 and phiSewage3 infected isolates of ST1, ST12, ST5, ST8, ST81, and ST88; the ΦETA2-like phages phiJP42 and phiJP43 infected isolates of ST1,

ST5, ST8, ST12, ST25, ST30, ST45, ST81, ST88, and ST89; and phiMW2 infected isolates of ST1, ST5, ST8, ST22, ST25, ST30, ST45, and ST88.

For descriptive purposes, 14 of the 16 STs were divided into two phenotypic groups based on their overall host range profiles (Supplementary Fig. 1). Group A (ST15, ST20, ST22, ST25, ST30, ST121, ST188, and ST764) showed a tendency toward phage resistance, with each strain susceptible to fewer than five of the tested phages. In contrast, Group B (ST5, ST8, ST45, ST81, ST88, and ST89) was broadly susceptible, with most strains susceptible to five or more phages. The remaining two STs, ST1 and ST12, were not assigned to either group because their isolates spanned both susceptibility patterns, and they are shown separately in Supplementary Fig. 1. However, even within a single ST, the number and identity of infecting phages varied among isolates (Supplementary Fig. 1), indicating that the clonal background alone does not predict susceptibility.

To examine whether antiphage defense repertoires contribute to this intralineage heterogeneity, we compared the number of predicted defense systems per genome with the number of infecting phages (Supplementary Fig. 2A). Across the 58 strains, the defense system content showed a weak but significant negative association with the number of infecting phages ($r = -0.45$, $P = 0.00045$). Consistent with this overall trend, within ST5 (n = 7) and ST89 (n = 4), strains with more defense systems tended to be infected with fewer phages (Supplementary Fig. 2B).

Although antiphage defense systems were broadly distributed across both Group A and B isolates, type II RM systems were enriched in Group A (ST15, ST20, ST25, ST121, and ST188; Supplementary Fig. 1). Within Group B, several isolates with stronger phage resistance than other strains of the same ST carried additional defense systems; for example, JP007 (ST89) encoded Gabija, Paris, and Wadjet, and JP182 (ST81) encoded an FS system. This observation led us to focus on lineage-matched susceptible and non-susceptible strains for candidate system discovery.

In CC5 (ST5/ST764), we identified two contrasting phenotypes (Fig. 2A). Three strains (JP090, JP091, and JP093), designated phage-susceptible CC5 (PSC5), were susceptible to multiple temperate phages, including the *eta*-carrying phages phiJP42, phiJP43, and phiJP72. In contrast, seven strains, designated phage-non-susceptible CC5 (PNC5), were resistant to most of the tested phages. Notably, all seven PNC5 strains carried two predicted antiphage defense systems, *stk2* and the *mad1*-like operon, that were absent from the three PSC5 strains.

To independently validate the association between *stk2*/*mad1*-like content and phage resistance, we expanded the analysis to an additional 25 CC5 strains: 12 strains lacking both systems (*stk2*-/*mad1*-; PSC5-candidate strains) and 13 strains carrying both systems (*stk2*+, *mad1*+; PNC5-candidate strains) (Fig. 2B, Supplementary Fig. 3, Supplementary Table 5).

Among the 12 PSC5-candidate strains (*stk2*-/*mad1*-), six strains were broadly susceptible to *eta*-carrying temperate phages (phiSewage2, phiSewage3, phiJP42, phiJP43, and phiJP72), whereas the remaining six strains showed resistance to these temperate phages. Of these six resistant strains, three carried

additional defense systems that may explain their reduced susceptibility despite the absence of *stk2* and *mad1*-like (Fig. 2B); strains 13008-19-S004 and JP095 encoded PD-T4-9_C, and 01040-19-S087 encoded AbiD (Supplementary Table 5). The remaining three strains, 46001-19-S048, 10019-19-S032, and JP098, lacked additional identifiable defense systems yet remained phage-resistant, indicating that determinants other than those detected by DefenseFinder contribute to the resistant phenotype in these strains. In contrast, 12 of the 13 PNC5-candidate strains were resistant to most tested phages, except phiJP152 and phiSewage6 (Fig. 2B, Supplementary Fig. 3), which was consistent with the broad phage resistance observed in the initial seven PNC5 strains (Fig. 2A). The mean plaque count across all tested phages was 80-fold higher in the PSC5-candidate strains than in the PNC5-candidate strains ($P = 0.025$). Together, these results suggest that defense system content, rather than CC5 lineage membership per se, accounts for the susceptibility difference within CC5, and that CC5 strains carrying both *stk2* and the *mad1*-like operon are resistant to multiple VF-encoding temperate phages.

Phage adsorption does not explain CC5-specific variation in phage susceptibility

To assess whether differences in phage adsorption could account for the CC5-specific variation in phage susceptibility, we performed adsorption assays using the laboratory strain RN4220 and 10 CC5 clinical isolates used in the host-range assay (Fig. 2A), using phage 80α (Fig. 3A): RN4220 adsorbed 81.3 ± 8.3% of phage particles, and most CC5 isolates showed even higher adsorption efficiencies (> 90%); the notable exceptions were JP093 (PSC5) and JP126 (PNC5), which adsorbed 64.8 ± 31.9% and 68.0 ± 24.7% of phage particles, respectively. A similar pattern was observed for phiJP42 (Fig. 3B), where RN4220 adsorbed 91.4 ± 3.8% of phage particles, most CC5 isolates again exceeded 90%, and JP093 and JP126 again fell below this range (75–85% adsorption). Significant overall differences were detected by the Kruskal–Wallis test for both 80α ($P = 0.0229$) and phiJP42 ($P = 0.0325$); however, subsequent pairwise Mann–Whitney *U* tests with Holm correction showed no significant differences between individual groups (all adjusted $P > 0.05$). The two strains with the lowest adsorption efficiencies belonged to different groups (JP093 in PSC5 and JP126 in PNC5) and thus did not track with the host-range phenotype. These results suggest that the CC5-specific difference in phage susceptibility between the PSC5 and PNC5 strains is unlikely to be explained by adsorption alone.

stk2 and mad1-like operon are located on distinct MGEs

To define the genomic context of *stk2* and the *mad1*-like operon, we compared the complete closed genomes of two CC5 strains, JP140 (ST5) and JP150 (ST764), with the draft genomes of the CC5 strains used in our host-range assay. In all the PNC5 strains, the *stk2* locus was mapped within the SCC*mec* type II element immediately adjacent to the SCC*mec* direct repeat (Fig. 4A). In contrast, the *mad1*-like operon was located within a *tst-1* carrying SaPI-associated locus (Fig. 4B). The *mad1*-like operon was located between the *S. aureus* chaperonin genes *groES–groEL*, immediately adjacent to a phage integrase gene. The surrounding region also contained the terminase small subunit gene *terS* and other SaPI-associated genes, suggesting that the operon is carried within an SaPI-related mobile element. Together, *stk2* and

mad1-like loci are encoded on two distinct MGEs, SCC*mec* and an SaPI-related element, rather than as part of the CC5 core chromosome.

To investigate whether the *mad1*-like operon is restricted to CC5 or is distributed more broadly, we screened 21,509 publicly available *Staphylococcaceae* genomes for *mad1*-like homologs. Mad1-like proteins and similar operons were detected in 3,144 genomes (~ 15%; Supplementary Table 6), spanning multiple *Staphylococcus* species (*S. epidermidis*, *S. argenteus, S. haemolyticus*, and others) and multiple STs of *S. aureus* (including ST30, ST36, ST45, and ST398). In *S. aureus*, *stk2* and the *mad1*-like operon co-occurred in both CC5 (ST5/ST764) and ST36 genomes (Supplementary Fig. 4A).

Across the 3,144 *mad1*-like positive genomes, the operon was in almost all cases positioned adjacent to a phage integrase gene and inserted between the chaperonin *groES–groEL* (Supplementary Fig. 4B).

stk2 and the mad1-like operon confer post-adsorption resistance to multiple VF-carrying phages

Because all the PNC5 strains carried both *stk2* and the *mad1*-like operon, we tested whether these two loci were sufficient to account for the reduced phage susceptibility of the PNC5 strains. The Stk2 protein encoded by the CC5 strain shares 100% amino acid identity with the previously characterized *S. epidermidis* Stk2 protein, suggesting functional conservation. The Mad1-like locus comprises a three-gene operon (*orf1–orf3*) encoded on the same strand (Fig. 5A and Supplementary Table 7): *orf1* encodes a Cro/C1-type helix–turn–helix (HTH) DNA-binding domain (PF01381); *orf2* encodes a protein with an HTH domain group 17 (PF12728); and *orf3* encodes a putative membrane-associated protein with a predicted signal peptide and transmembrane helix (Supplementary Table 7).

We cloned *stk2* or the *mad1*-like operon, together with their predicted native promoter, into the shuttle vector pLI50. Each construct was transformed into the restriction-deficient laboratory strain *S. aureus* RN4220, which lacked both systems and was susceptible to the tested phages. The efficiency of plating (EOP) values shown in Fig. 5B and C are expressed relative to the empty vector control. Compared with RN4220 cells carrying the empty pLI50 vector, expression of either *stk2* or the *mad1*-like operon reduced the EOP of multiple temperate phages, including the *eta*-carrying phages phiJP42, phiJP43, and phiJP72, approximately 10^2- to 10^7-fold (Fig. 5B). In addition, expression of the *mad1*-like operon, but not *stk2*, reduced the EOP of phiUSA300 10^2-fold and produced a small-plaque phenotype in phiJP42, phiJP43, and phiJP49 (Fig. 5B and Supplementary Fig. 5). To confirm that the activities of *stk2* and the *mad1*-like operon were not specific to the laboratory genetic background of RN4220, we introduced each construct into JP090, a CC5 strain belonging to the PSC5 group that naturally lacks both systems. In JP090, the expression of *stk2* or the *mad1*-like operon also reduced the EOP of *eta*-carrying phages (phiJP42, phiJP43, and phiJP72) and phiJP152 10- to 10^7-fold (Fig. 5C). Notably, phiJP152 retained the ability to form plaques on native PNC5 strains (Fig. 2B and Supplementary Fig. 3) despite being restricted by *stk2* and the *mad1*-like operon when these were expressed from a plasmid in JP090, suggesting that the level of expression of these systems influences the outcome of infection by phiJP152. To clarify whether the EOP reduction was due to reduced phage adsorption or post-adsorption inhibition, we quantified the

adsorption efficiency of phiJP42 to RN4220 derivative strains. Adsorption rates were similarly high across all three strains: 95.3 ± 2.9% for RN4220_pLI50, 93.7 ± 2.5% for RN4220_pLI50-*stk2*, and 99.3 ± 0.1% for RN4220_pLI50-*mad1*-like operon (Fig. 5D). The Kruskal–Wallis test indicated a significant overall difference ($P = 0.0496$); however, subsequent pairwise Mann–Whitney *U* tests with Holm correction did not identify any significant pairwise differences (all adjusted $P > 0.05$).

Some antiphage defense systems are induced upon phage infection, whereas others are constitutively expressed [25]. To determine which mode applies to *stk2* and the *mad1*-like operon, we quantified their transcript levels in JP145 (PNC5) by reverse transcription quantitative PCR (RT-qPCR) at 30 min post-infection with 80α and phiJP42 (Supplementary Fig. 6). Relative to the no-phage condition, *mad1*-like transcript levels were 0.6 ± 0.3-fold for phiJP42 and 1.3 ± 0.4-fold for 80α, and *stk2* transcript levels were 0.9 ± 0.4-fold for phiJP42 and 0.7 ± 0.2-fold for 80α. None of these changes was statistically significant between infected and uninfected conditions for either system (Mann–Whitney *U* test with Holm correction: *stk2*: phiJP42, $P = 0.39$; 80α, $P = 0.18$; *mad1*-like: phiJP42, $P = 0.05$; 80α, $P = 0.48$).

Taken together, these results suggest that differences in phage susceptibility among CC5 strains are influenced more strongly by defense systems such as Stk2 and the Mad1-like system than by adsorption efficiency.

Discussion

In this study, we demonstrated that strain-specific antiphage defense systems are important determinants of host permissiveness to VF-carrying temperate phages in *S. aureus*. By combining the isolation and genomic characterization of 11 temperate phages with host-range profiling across 58 clinical isolates spanning 16 STs, together with functional validation of candidate defense systems in two genetic backgrounds, we demonstrated that susceptibility to VF-carrying temperate phages varies both between and within lineages and that this variation is shaped, at least in part, by mobile, strain-specific defense systems. Together with our recent identification of the lineage-specific defense factor SadR, these findings support a hierarchical model in which both lineage- and strain-specific intracellular defense systems collectively shape host permissiveness to MGEs in *S. aureus*. In the CC5 lineage, *stk2* and the *mad1*-like operon are each sufficient to confer resistance to multiple temperate phages, including five *eta*-carrying phages, and act after phage adsorption without infection-dependent induction. These findings extend the longstanding view that the susceptibility of *S. aureus* to temperate phages is primarily determined by WTA-mediated adsorption, revealing that intracellular mobile defense systems constitute the second layer governing host permissiveness after phage adsorption.

Most prior studies on antiphage defense systems have emphasized the molecular mechanisms by which individual systems inhibit phage infection [26, 27], and have established the central role of RM systems in the lineage-specific blocking of MGE acquisition in *S. aureus* [28, 29]. In contrast, the broader question regarding how diverse non-RM defense systems shape the dissemination of clinically important MGEs, particularly those carrying VFGs and ARGs, has received less attention [30]. Because antiphage defense

systems are often encoded on MGEs, such as prophages, SaPIs, integrons, plasmids, and SCC elements [31, 32, 33], they constitute part of the accessory genome and produce strain-dependent defense repertoires. Our work links this strain-level variation in defense system content to differential susceptibility to VF-carrying temperate phages and identifies two specific systems, *stk2* and the *mad1*-like operon, that operate in CC5 strains. More broadly, our findings suggest that antiphage defense repertoires are organized at multiple evolutionary scales, with lineage-associated defense systems appearing to define broad MGE permissiveness, and mobile accessory defense systems generating heterogeneity among strains within individual lineages.

The lineages we classified as Group A (ST15, ST20, ST22, ST25, ST30, ST121, ST188, and ST764; Supplementary Fig. 1) showed reduced phage susceptibility, and most of them (ST15, ST20, ST25, ST30, ST121, and ST188) also carried a lower burden of ARGs and were predominantly methicillin-susceptible (Supplementary Table 4). For these lineages, the co-occurrence of low phage susceptibility and low ARG burden is consistent with a generally reduced permissiveness to MGEs, including SCC*mec*, plasmids, and temperate phages. Two Group A lineages, ST22 and ST764, are exceptions: all isolates of both lineages in our panel were *mecA*-positive (Supplementary Table 4). In ST764, reduced phage susceptibility is instead attributable to the mobile defense systems described here, one of which, *stk2*, is itself carried within the SCC*mec* type II element. Low phage susceptibility and MGE acquisition are therefore not strictly coupled, and a lineage can combine a resistant phage phenotype with an MRSA background.

Group A also includes several clinically important MSSA ST lineages; ST15 and ST121 are well-known for harboring ETA-positive strains [34, 35], and ST121 also includes PVL-positive isolates [36, 37]. Notably, three *eta*-carrying phages characterized here were themselves induced from Group A donor strains: phiJP72 from an ST15 isolate and phiSewage2 and phiSewage3 from ST121 isolates (Supplementary Table 1). These lineages are therefore permissive to *eta*-carrying phages as prophage carriers, yet none of the ST15 or ST121 isolates in our host-range panel were productively infected by these same phages. Two non-exclusive explanations are consistent with this pattern. First, superinfection immunity conferred by resident homoimmune prophages would block productive infection in isolates that already carry a related element, which is the expected situation for ETA-positive ST15 and ST121 strains [12, 20]. Second, *eta* in these STs may have been acquired by an ancestral progenitor and subsequently maintained largely by vertical transmission [20, 34], rather than by ongoing horizontal acquisition. Distinguishing between these possibilities would require testing *eta*-negative, prophage-cured derivatives of ST15 and ST121 isolates, which was beyond the scope of the present study.

The molecular basis underlying the low MGE permissiveness of Group A lineages is beginning to emerge. A recently characterized defense factor, SadR, is present in the large majority of methicillin-susceptible ST188 strains and encodes an HEPN-type RNase that restricts phage infection and plasmid transformation [18]. *sadR* is located immediately downstream of the ribosomal RNA large subunit methyltransferase H gene *rlmH*, the SCC*mec* integration site, suggesting that it may directly impede the first step of MRSA emergence. Our previous identification of SadR indicated that lineage-specific

defense systems could contribute to the establishment of a low-permissiveness genetic background for MGE acquisition. The present study extends this concept by identifying additional mobile defense systems such as *stk2* and the *mad1*-like operon, which further diversify host permissiveness among strains within a single lineage. Whether analogous lineage-specific defense systems contribute to the low MGE burden in other Group A lineages, such as ST15, ST20, ST25, and ST121, remains an open and important question. Taken together, these observations support a hierarchical model for host permissiveness in *S. aureus*. Lineage-specific defense systems, exemplified by SadR, appear to establish the overall propensity of a lineage to acquire MGEs. In contrast, strain-specific defense systems, such as *stk2* and the *mad1*-like operon, contribute to the heterogeneity in permissiveness among closely related strains. The two classes of system also differ in how they are distributed. *sadR* is largely fixed within the ST188 lineage (76.7% of the isolates examined, 148/193)[18], with a minor cluster lacking *sadR*, most members of which are clonally related strains isolated from the same hospital in Vietnam[38]. Contrary, *stk2* and the *mad1*-like operon are carried on mobile elements and are present in only a subset of strains within CC5. We therefore use “lineage-specific” and “strain-specific” to describe the predominant distribution pattern of each class, rather than to imply that either is strictly confined to a single genetic level. This hierarchical organization provides a conceptual framework for understanding why MGE content varies not only between lineages, but also among strains belonging to the same clonal lineage.

Group B lineages (e.g., ST8 and ST88), which include epidemic community-associated MRSA clones, such as USA300 [39], were broadly susceptible to multiple temperate phages, consistent with their higher permissiveness to phage-mediated acquisition of VF and other accessory genes [40].

Stk2 has previously been characterized in *S. epidermidis* as a serine/threonine kinase that is activated by the phage protein PacK and triggers host-cell death [41]. Our data showed that Stk2 restricted multiple VF-carrying *S. aureus* phages, including phiJP42, phiJP43, and phiJP72. These results extend the documented activity of Stk2 to clinically relevant VF-carrying temperate phages in *S. aureus*.

The *mad1*-like operon identified in this study is related to *mad1*, a component of the MADS operon (Mad1–Mad6) originally described in *Pseudomonas aeruginosa*, in which Mad1 contains an HTH DNA-binding domain [42]. The CC5 *mad1*-like operon encodes proteins with HTH- and excisionase-like domains, suggesting that the system interacts with DNA or other nucleic acids [43]. Notably, the *mad1*-like operon is located immediately adjacent to an SaPI-associated integrase in a region typically occupied by SaPI repressor/anti-repressor genes [44]. Repressor/anti-repressor modules in this region govern the induction and mobilization of prophages and SaPIs [45, 46], and SaPI-encoded transcriptional repressors have been shown to mediate antiphage defense [47]. Taken together, these observations suggest that this region may serve as a hotspot for both mobile element life cycle control and antiphage defense. However, a direct functional association between the SaPI repressor/anti-repressor and the *mad1*-like operon remains to be established experimentally. Although we attempted to identify the gene responsible for antiphage defense activity within the *mad1*-like operon, we were unable to obtain transformants carrying plasmids expressing each gene individually (only *orf1* could be stably maintained). One explanation is that the

operon encodes a toxin-antitoxin-like arrangement, in which expression of an effector in the absence of its cognate partner is not tolerated by the host, a configuration described for several characterized antiphage defense systems. Consistent with this, *orf1* encodes a Cro/C1-type HTH DNA-binding protein (Supplementary Table 7) and was the only gene that could be stably maintained on its own. However, further studies are needed to clarify the mechanism underlying its antiphage activity.

Our finding that *stk2* resides within the SCC*mec* type II element is consistent with a recent report showing that staphylococcal antiphage defense systems are frequently encoded within or adjacent to SCC*mec* cassettes, and that SCC*mec*-encoded recombinases can mobilize tandem SCC-like cassettes enriched in defense genes[33]. Our data extend this observation by demonstrating that an SCC*mec*-borne defense system restricts VF-encoding temperate phages in clinical isolates, and by showing that a second, independently mobile defense system, the *mad1*-like operon, acts in the same strains. Together, these findings suggest that the SCC*mec* locus serves not only as the determinant of methicillin resistance but also as a reservoir and vehicle for antiphage immunity.

Our study had some limitations. First, the causal role of *stk2* and the *mad1*-like operon rests on gain-of-function experiments in two naive backgrounds, RN4220 and the PSC5 strain JP090. Repeated attempts to delete either locus in native PNC5 strains were unsuccessful, failing at the transformation step (Methods), so the necessity of these loci in their native background remains to be established. Second, the causal role of both systems was demonstrated primarily in the CC5 lineage, and whether similar strain-specific defense modules account for variation in host permissiveness in other *S. aureus* CCs requires further functional studies. Third, our adsorption assays ruled out differences at the pre-adsorption level but did not resolve the precise post-adsorption step targeted by *stk2* or the *mad1*-like operon. Further experiments are needed to determine whether replication, transcription, packaging, or other stages are restricted. Fourth, as noted above, we were unable to express individual ORFs of the *mad1*-like operon under our experimental conditions, which precluded fine dissection of the genetic determinants of its antiphage activity and identification of the catalytic component.

In conclusion, our findings established strain-specific mobile antiphage defense systems, exemplified by *stk2* on the SCC*mec* type II element and the *mad1*-like operon within an SaPI-related region of the CC5 lineage, as key modulators of host permissiveness to VF-carrying temperate phages in *S. aureus*. Together with our previous identification of the lineage-specific defense factor SadR, the present study suggests that host permissiveness to VF-encoding temperate phage is hierarchically organized through both lineage-specific and strain-specific intracellular defense systems. This multilayered defense architecture provides a conceptual framework for understanding lineage- and strain-dependent heterogeneity in susceptibility to VF-encoding temperate phages in *S. aureus*.

Materials and Methods

Bacterial strains and growth media

All cultures were grown at 37°C with shaking at 200 rpm, unless otherwise stated. *S. aureus* RN4220, a restriction-deficient strain [48], was used as the recipient for transformation and maintenance of recombinant plasmids. *S. aureus* strains were routinely grown in tryptic soy broth (TSB) or on agar (TSA) plates (Becton Dickinson and Company, Franklin Lakes, NJ, USA). Phage susceptibility assays were performed using the double-agar overlay method, in which TSB containing 0.6% (w/v) agar (hereafter referred to as soft agar) was overlaid onto TSA plates. Chloramphenicol was added at 10 μg/mL when required. *Escherichia coli* DH5α competent cells (Takara Bio Inc., Shiga, Japan) were used for plasmid construction and maintenance. They were cultured in Luria–Bertani (LB) broth or LB agar (Becton, Dickinson and Company, Franklin Lakes, NJ, USA), supplemented with ampicillin (100 μg/mL) for plasmid selection. The reference strains MW2[49] and USA300[50] were included in the host-range panel and as prophage donors.

Prophage induction and phage isolation

A total of 254 *S. aureus* isolates were screened for mitomycin C-inducible prophages, comprising 199 clinical, 29 sewage-derived, and 26 companion animal isolates. The isolated metadata are provided in Supplementary Table 1. Overnight cultures of each isolate were diluted 1:1,000 into 20 mL of fresh TSB and incubated at 37°C with shaking until the optical density at 600 nm (OD_{600}) reached 0.2–0.3. Prophage induction was initiated by adding mitomycin C (Nacalai Tesque, Kyoto, Japan) to a final concentration of 1 μg/mL, followed by incubation for 5 h at 37°C with shaking at 180 rpm. Cultures were centrifuged at 10,000 × *g* for 15 min, and the supernatants were filtered through a 0.22-μm membrane (Merck Millipore, Burlington, MA, USA) to obtain phage lysates. Phage-containing lysates were recovered from 39 of the 254 isolates (22 clinical, nine sewage-derived, and eight companion animal isolates).

Phage titers were determined using 10-fold serial dilutions in phosphate-buffered saline PBS (Nippon Gene Co., Ltd., Tokyo, Japan). Single plaques were selected, resuspended in 100 μL of TSB, and incubated at 37°C for 1–2 h. After centrifugation at 19,000 × *g* for 5 min, the supernatants were spotted onto a soft agar lawn of RN4220 to isolate single plaques, which was performed at least twice for each phage. Purified phages were propagated on RN4220 as the indicator strain, and lysates with sufficient titers were used to extract genomic DNA and perform whole-genome sequencing. High-quality genomic sequences were obtained for 11 distinct phages and used in subsequent analyses.

Phage susceptibility spot assay

S. aureus RN4220, its plasmid-carrying derivatives, and clinical isolates were grown overnight in TSB at 37°C, with chloramphenicol (10 μg/mL) added for plasmid-carrying strains. Molten soft agar (10 mL, held at 50°C) was mixed with 100 μL of culture and $CaCl_2$ (10 mM final concentration) and poured over a TSA plate. Phage lysates were diluted 10-fold in PBS in 96-well plates, and 2.5 μL of each dilution was spotted onto the solidified overlay. Once the spots had dried, the plates were incubated at 37°C without

agitation and read for plaques after 18–24 h. Every strain–phage combination was tested at least three times.

Efficiency of plating (EOP)

Plating efficiencies were measured on RN4220 or JP090 carrying pLI50-*mad1*-like or pLI50-*stk2*, and referenced to the corresponding host carrying the empty pLI50 vector. Cultures and overlays were prepared as described above on TSA containing chloramphenicol (TSA-CP10). Reference and test hosts were plated on the same day from a single dilution series of each lysate. Plaques were counted in the spots at the highest dilution, giving discrete plaques, titers were converted to plaque-forming unit (PFU) per mL, and EOP was taken as the titer on the test host over that on RN4220 (pLI50). Means ± SD of three independent experiments are shown, with comparisons made on $\log_{10}$-transformed titers. Phages whose plaques were too small to count on TSA-CP10 for both the reference and test hosts were excluded from the analysis and did not appear in the figures.

Phage DNA extraction, sequencing, and genome assembly

Phage genomic DNA was extracted using the phenol–chloroform (1:1, v/v) method. Briefly, 1 mL of phage lysate was treated with RNase A (final concentration, 10 µg/mL; Thermo Fisher Scientific, Waltham, MA, USA) and 2 µL (10 U) of DNase I (TaKaRa Bio, Shiga, Japan) and incubated at 37°C for 1 h to degrade contaminating nucleic acids. The reaction was stopped by adding 15 µL of 0.5 M EDTA, after which 4 µL of 20% SDS and 2 µL (1.2 U) of proteinase K (Nacalai Tesque, Kyoto, Japan) were added. The mixture was incubated at 55°C for 2 h with shaking at 2,000 rpm to lyse the phage capsids and digest proteins.

DNA was purified by phenol–chloroform extraction (1:1, v/v). After each extraction, samples were centrifuged at 16,000 × *g* for 3 min, and the aqueous phase was transferred to a new tube. DNA was precipitated by adding 0.1 volume of 3 M sodium acetate and 2.5 volumes of ice-cold 100% ethanol, then incubating at − 20°C for at least 30 min.

DNA pellets were collected by centrifugation at 16,000 × *g* for 30 min, washed twice with 70% ethanol, air-dried, and resuspended in 30 µL of sterile ddH_2O. Phage DNA library was prepared using the QIA seq FX DNA library kit (Qiagen, Hilden, Germany), and sequencing was performed on the Illumina MiSeq platform. Short-read *de novo* assembly was performed using Shovill v1.1.0 (https://github.com/tseemann/shovill) with SPAdes [51] as the assembler (--minlen 500). Genome annotation was carried out using Pharokka v1.7.5 [52]. Assembled phage genomes were reoriented using dnaapler v1.2.0 [53] in custom mode, with the terminase small subunit gene *terS* used as the starting reference.

Phage phylogenetic analysis and genome visualization

For phage phylogenetic analysis, a viral proteomic tree was constructed using ViPTree with the 11 phage genomes obtained in this study, together with 193 *Staphylococcus* phage reference genomes retrieved from the ViPTree database (accessed on February 25, 2026) [54]. The resulting tree was visualized and annotated using iTOL v7.5 [55]. Metadata displayed on the tree included genome length, predicted phage lifestyle, and the presence or absence of VFGs for each phage. Phage lifestyle was predicted using PhaBOX [56]. VFs were identified using a custom in-house database curated for the detection of *S. aureus*-associated VFGs [17]. Phage genomic similarity was calculated using VIRIDIC (https://rhea.icbm.uni-Oldenburg.de/viridic/).

Genomic DNA extraction and sequencing of S. aureus

Genomic DNA was extracted from *S. aureus* as previously described, with minor modifications [17]. Briefly, isolates were streaked from glycerol stocks onto TSA plates and incubated overnight at 37°C. A single colony was inoculated into 5 mL of TSB and cultured at 37°C for 12 h. Bacterial cells were harvested by centrifugation at 8,000 × *g* for 2 min and resuspended in 200 µL of CS buffer (50 mM Tris-HCl [pH 7.5], 10 mM EDTA, and 150 mM NaCl).

To digest the cell wall and remove RNA, 2 µL of lysostaphin (5 mg/mL, FUJIFILM Wako Pure Chemical Corporation, Osaka, Japan) and 1 µL of RNase A (10 mg/mL) were added, followed by incubation at 37°C for 30 min. Subsequently, 20 µL of 20% SDS and 10 µL of proteinase K (50 mg/mL; Nacalai Tesque, Kyoto, Japan) were added, and the mixture was incubated at 55°C for 2 h to lyse the cells and degrade proteins. Genomic DNA was then purified using Agencourt AMPure XP beads (Beckman Coulter, Brea, CA, USA) according to the manufacturer's instructions. The purified DNA was finally dissolved in 20 µL of sterile distilled water and stored at − 30°C until use.

Bioinformatics analysis

ARGs were detected using ABRicate v1.0.1 (https://github.com/tseemann/abricate) with the ResFinder database (updated on September 5, 2024), applying thresholds of ≥ 80% identity and ≥ 80% coverage [57]. VFs were identified using an in-house database developed for more precise detection of *S. aureus*-specific VFs [17]. Candidate defense genes were selected based on the HMMER output generated by DefenseFinder v1.2.2 [23, 58]. No *E*-value cutoff was applied at the discovery stage to maximize sensitivity, and candidate defense systems were retained for downstream analysis only if they were identified using DefenseFinder default thresholds in at least one closed reference genome. To detect Mad1-like proteins in other species, we collected amino acid and genome sequences using ncbi-genome-download (https://github.com/kblin/ncbi-genome-download) v0.3.1, focusing on members of the *Staphylococcaceae* and including representative outgroup genera (total n = 21,509). The collected sequences were analyzed using local BLASTP v2.12, with default *E*-value settings, using the Mad1-like protein as the query and applying thresholds of ≥ 80% identity and ≥ 80% query coverage. A core-genome alignment against strains harboring the Mad1-like defense system was generated using Roary [59] with slightly relaxed thresholds to accommodate the multispecies dataset (parameters: -cd 95–i 80). SNPs

were extracted from the alignment using SNP-sites [60]. A phylogenetic tree was inferred from the core-genome SNP alignment using FastTree v2.2 [61] under the GTR + Γ model and visualized using iTOL v7.5 [55]. A 10-kb region flanking the *mad1*-like gene on both sides was extracted from assemblies in which the locus was contiguous, and representative genomes were visualized using Clinker v0.0.28 (https://github.com/gamcil/clinker).

The deduced amino acid sequence of the *mad1*-like gene product from strain JP145 was analyzed using InterProScan 5 (default settings; accessed on February 26, 2026) [62] to predict functional domains and protein family assignments.

Adsorption Assay

S. aureus clinical isolates (Supplementary Table 5) and plasmid-transformed RN4220 and JP strains carrying the empty pLI50 vector, pLI50-*mad1*-like, or pLI50-*stk2* were grown overnight without shaking at 37°C in TSB. Overnight cultures (30 µL) were inoculated into 3 mL of fresh TSB containing 10 mM $CaCl_2$ (1:100 dilution) and incubated at 37°C with shaking until the optical density at 600 nm (OD_{600}) reached approximately 0.5. For clinical isolates, phages 80α and phiJP42 were added at multiplicity of infections (MOIs) of 0.1 (1.0×10^7 PFU) and 0.01 (1.0×10^6 PFU), respectively. For plasmid-transformed strains, phiJP42 was added at an MOI of 0.1. The mixtures were incubated at 37°C for 10 min without shaking to allow phage adsorption, then immediately centrifuged at 13,000 × *g* for 3 min at 4°C to pellet bacteria and adsorbed phages. Supernatant was then passed through 0.22-µm filters by centrifugation at 8,000 × *g* for 3 min at 4°C to remove any remaining bacteria. Unadsorbed phages in the filtrate were quantified by 10-fold serial dilutions in PBS and spot assays, using *S. aureus* RN4220 as the indicator strain.

Adsorption efficiency (%) was calculated using the following equation:

$$\text{Adsorption efficiency (\%)} = \frac{P_{\text{added}} - P_{\text{supernatant}}}{P_{\text{added}}} \times 100$$

where P_{added} is the initial number of phages added, and $P_{\text{supernatant}}$ is the number of phages remaining in the supernatant after incubation.

Construction of stk2- and mad1-complemented RN4220 strains

Upstream promoter regions of *stk2* and *mad1* were predicted using BPROM (SoftBerry, http://www.softberry.com/), and the corresponding gene regions were amplified by PCR using KOD FX Neo (TOYOBO, Osaka, Japan). Primers used are listed in Supplementary Table 9. The amplified fragments were cloned into the shuttle vector pLI50 [63] using the NEBuilder HiFi DNA Assembly Kit (New England Biolabs, Ipswich, MA, USA) according to the manufacturer's instructions. The assembled plasmids were then transformed into *E. coli* DH5α competent cells (Takara Bio Inc., Shiga, Japan) and selected on LB agar containing ampicillin (100 µg/mL).

Plasmids were purified from *E. coli* transformants using the Monarch Plasmid Extraction Kit (New England Biolabs, Ipswich, MA, USA) and verified by Sanger sequencing using the BigDye Terminator v3.1 Cycle Sequencing Kit (Applied Biosystems, Waltham, MA, USA).

Confirmed plasmids were introduced into *S. aureus* RN4220 and into the PSC5 strain JP090 by electroporation [64]. Following a 2 h recovery, cells were plated on TSA containing chloramphenicol (10 µg/mL). Chloramphenicol-resistant colonies were screened by PCR, and verified transformants were used as the *stk2*- and *mad1*-like-expressing strains in the plating efficiency and adsorption assays.

Attempted construction of deletion mutants

Allelic exchange constructs carrying the regions flanking *stk2* or the *mad1*-like operon were assembled in the temperature-sensitive *E. coli–S. aureus* shuttle vectors pKFC and pKFT[65]. For each recipient strain, the vector carrying the selectable marker to which that strain was susceptible was used. Constructs were verified by Sanger sequencing and introduced into PNC5 strains by multi-pulse electroporation[60], with all subsequent culture steps performed at the permissive temperature as described[65]. No transformants were recovered from any of the recipient strains tested, and deletion mutants were therefore not obtained.

RNA extraction

S. aureus strain JP145 was pre-cultured overnight in TSB. The overnight bacterial suspension was diluted 100-fold (30 µL into 3 mL of fresh TSB) and incubated at 37°C with shaking at 180 rpm until an OD_{600} of 0.5 was reached. Phage 80α or phiJP42 was then added at an MOI of 1, and the culture was further incubated at 37°C with shaking at 180 rpm for 30 min. Cells were harvested by centrifugation, and the pellet was washed twice with PBS. Washed cells were disrupted by bead beating twice for 45 s with a 5-min interval on ice using a FastPrep-24 5G instrument and Lysing Matrix B tubes (MP Biomedicals, Irvine, CA, USA). Total RNA was extracted using the NucleoSpin RNA kit (MACHEREY-NAGEL GmbH & Co. KG, Düren, Germany) according to the manufacturer's instructions. To remove residual genomic DNA, an additional DNase treatment was performed using RQ1 RNase-free DNase (Promega, Madison, WI, USA) after RNA purification. Purified RNA was used for downstream analyses.

Reverse transcription quantitative PCR

Total RNA was reverse transcribed into cDNA using PrimeScript™ IV 1st-Strand cDNA Synthesis Mix (Takara Bio, Shiga, Japan) according to the manufacturer's instructions. Quantitative real-time PCR was performed using primers targeting internal regions of the *stk2* and *mad1*-like genes, with *gyrB* as an internal control (Supplementary Table 9). Reactions were carried out using SsoAdvanced™ Universal SYBR® Green Supermix (Bio-Rad Laboratories, Hercules, CA, USA) with 0.25 µM of each primer in a final volume of 20 µL on a CFX96 Real-Time PCR Detection System (Bio-Rad Laboratories) under the following conditions: 95°C for 3 min, followed by 44 cycles of 95°C for 10 s and 55°C for 35 s. A melting curve analysis (65–95°C, 0.5°C increments) was performed to confirm amplification specificity. ΔCt values were calculated by normalizing to *gyrB* expression, and ΔΔCt values were calculated relative to

the mean ΔCt of the no-phage control, which served as the calibrator. Each sample was analyzed in technical triplicate across two independent biological replicates; one additional experiment was excluded due to marked inconsistencies in Ct values across targets and replicates.

Statistical analysis

All statistical analyses were performed in Python v3.12.4, using SciPy v1.13.1 and statsmodels v0.14.6. All tests were two-sided, and a *P*-value of < 0.05 was considered statistically significant. Groups of three or more were compared using the Kruskal–Wallis test, followed by pairwise comparisons using the Mann–Whitney *U* test with Holm correction for multiple testing. Comparisons of plaque counts between PSC5-candidate and PNC5-candidate strains were performed using the Kruskal–Wallis test, followed by pairwise Mann–Whitney *U* tests with Holm correction on $\log_{10}$-transformed counts. The association between the number of predicted defense systems and the number of infecting phages was assessed using the Pearson correlation coefficient. Relative transcript levels measured by RT-qPCR were compared between phage-exposed and unexposed conditions using the Mann–Whitney *U* test with Holm correction on ΔCt values.

Declarations

Data availability

The nucleotide sequences of the 11 phage genomes determined in this study have been deposited in the DNA Data Bank of Japan (DDBJ) under BioProject accession PRJDB42742 (sequence accession numbers DRR1092864 - DRR1092874). The bacterial host genome sequences newly determined in this study have been deposited under BioProject accession PRJDB43077. The individual Run accession numbers and BioSample numbers for the corresponding phages are listed in Supplementary Table 2. The individual accession numbers of *S. aureus* genome sequences used in this study are listed in Supplementary Tables 1, 4, and 5. All other data supporting the findings of this study are available within the Supplementary Materials.

Code availability

No custom codes were used in this study. All analyses were performed using publicly available software, as described in the Materials and Methods section, with the specified parameters.

Acknowledgements

This work was supported by the Japan Agency for Medical Research and Development (AMED) under grant numbers 24fk0108699j0001, 25fk0108699h0002, and 26fk0108699h0003 to M.S., and by the Japan Society for the Promotion of Science (JSPS) KAKENHI under grant number 25K20585 to K.Ko. Phage 80α was kindly provided by José R. Penadés (Imperial College London, UK). We thank all contributors who provided the *S. aureus* strains used in this study. We thank Noriko Sakamoto and Elahi Shahim for their technical assistance with sequencing.

Author contributions

Author initials are abbreviated as follows: S.K., Shoko Kutsuno; K.Ko., Kohei Kondo; Y.S., Yo Sugawara; A.A., Aa Haeruman Azam; K.Kg., Kotaro Kiga; K.I-K., Kasumi Ishida-Kuroki; M.K., Mitsuoki Kawano; S.Ka., Shizuo Kayama; M.T., Manami Tsunoi; M.M., Miyo Murai; K.Ki., Kozue Kishii; M.O., Makoto Ohnishi; M.S., Motoyuki Sugai; J.H., Junzo Hisatsune.

S.K. and K.Ko.: Conceptualization, Investigation, Formal analysis, Writing – original draft. K.Ko.: Funding acquisition. M.T. and K.I-K.: Investigation, Formal analysis. A.A., K.Kg., and M.K.: Investigation, Data curation, Writing—review & editing. S.Ka., M.M., and K.Ki.: Investigation, Resources. Y.S.: Investigation. M.O.: Supervision, Writing—review & editing. M.S. and J.H.: Conceptualization, Funding acquisition, Supervision, Writing—review & editing. All authors read and approved the final manuscript.

Competing interests

The authors declare no competing interests.

References

1. Tong SY, Davis JS, Eichenberger E, Holland TL, Fowler VG (2015) Jr. Staphylococcus aureus infections: epidemiology, pathophysiology, clinical manifestations, and management. Clin Microbiol Rev 28:603–661. https://doi.org/10.1128/CMR.00134-14
2. Hennekinne JA, De Buyser ML, Dragacci S (2012) Staphylococcus aureus and its food poisoning toxins: characterization and outbreak investigation. FEMS Microbiol Rev 36:815–836. https://doi.org/10.1111/j.1574-6976.2011.00311.x
3. Cheung GYC, Bae JS, Otto M (2021) Pathogenicity and virulence of Staphylococcus aureus. Virulence 12:547–569. https://doi.org/10.1080/21505594.2021.1878688
4. Grumann D, Nubel U, Broker BM (2014) Staphylococcus aureus toxins–their functions and genetics. Infect Genet Evol 21:583–592. https://doi.org/10.1016/j.meegid.2013.03.013
5. Ladhani S, Joannou CL, Lochrie DP, Evans RW, Poston SM (1999) Clinical, microbial, and biochemical aspects of the exfoliative toxins causing staphylococcal scalded-skin syndrome. Clin Microbiol Rev 12:224–242. https://doi.org/10.1128/cmr.12.2.224
6. Bukowski M, Wladyka B, Dubin G (2010) Exfoliative toxins of Staphylococcus aureus. Toxins (Basel) 2:1148–1165. https://doi.org/10.3390/toxins2051148
7. Nishifuji K, Sugai M, Amagai M (2008) Staphylococcal exfoliative toxins: molecular scissors of bacteria that attack the cutaneous defense barrier in mammals. J Dermatol Sci 49:21–31. https://doi.org/10.1016/j.jdermsci.2007.05.007
8. Lina G et al (1999) Involvement of Panton-Valentine leukocidin-producing Staphylococcus aureus in primary skin infections and pneumonia. Clin Infect Dis 29:1128–1132. https://doi.org/10.1086/313461

9. Jhelum H et al (2024) Panton-Valentine leukocidin-induced neutrophil extracellular traps lack antimicrobial activity and are readily induced in patients with recurrent PVL + -Staphylococcus aureus infections. J Leukoc Biol 115:222–234. https://doi.org/10.1093/jleuko/qiad137
10. Labandeira-Rey M et al (2007) Staphylococcus aureus Panton-Valentine leukocidin causes necrotizing pneumonia. Science 315:1130–1133. https://doi.org/10.1126/science.1137165
11. Gillet Y et al (2002) Association between Staphylococcus aureus strains carrying gene for Panton-Valentine leukocidin and highly lethal necrotising pneumonia in young immunocompetent patients. Lancet 359:753–759. https://doi.org/10.1016/S0140-6736(02)07877-7
12. Ingmer H, Gerlach D, Wolz C (2019) Temperate Phages of Staphylococcus aureus. Microbiol Spectr 7. https://doi.org/10.1128/microbiolspec.GPP3-0058-2018
13. Rohmer C et al (2022), *Influence of Staphylococcus aureus Strain Background on Sa3int Phage Life Cycle Switches. Viruses 14.* https://doi.org/10.3390/v14112471
14. Chaguza C et al (2022) Prophage-encoded immune evasion factors are critical for Staphylococcus aureus host infection, switching, and adaptation. Cell Genom 2. https://doi.org/10.1016/j.xgen.2022.100194
15. Malachowa N, DeLeo FR (2010) Mobile genetic elements of Staphylococcus aureus. Cell Mol Life Sci 67:3057–3071. https://doi.org/10.1007/s00018-010-0389-4
16. Souza SSR et al (2024) Demographic fluctuations in bloodstream Staphylococcus aureus lineages configure the mobile gene pool and antimicrobial resistance. NPJ Antimicrob Resist 2:14. https://doi.org/10.1038/s44259-024-00032-9
17. Hisatsune J et al (2025) Staphylococcus aureus ST764-SCCmecII high-risk clone in bloodstream infections revealed through national genomic surveillance integrating clinical data. Nat Commun 16:2698. https://doi.org/10.1038/s41467-025-57575-2
18. Kondo K et al (2026) RNase-mediated defence and its association with SCCmec in Staphylococcus aureus. Nat Commun. https://doi.org/10.1038/s41467-026-75971-0
19. Brown S, Santa Maria JP Jr., Walker S (2013) Wall teichoic acids of gram-positive bacteria. Annu Rev Microbiol 67:313–336. https://doi.org/10.1146/annurev-micro-092412-155620
20. Xia G, Wolz C (2014) Phages of Staphylococcus aureus and their impact on host evolution. Infect Genet Evol 21:593–601. https://doi.org/10.1016/j.meegid.2013.04.022
21. Beck C et al (2024), *Wall teichoic acid substitution with glucose governs phage susceptibility of Staphylococcus epidermidis. mBio 15, e0199023* https://doi.org/10.1128/mbio.01990-23
22. Kuijk MM et al (2025), *The two-component system ArlRS is essential for wall teichoic acid glycoswitching in Staphylococcus aureus. mBio 16, e0266824* https://doi.org/10.1128/mbio.02668-24
23. Tesson F et al (2022) Systematic and quantitative view of the antiviral arsenal of prokaryotes. Nat Commun 13:2561. https://doi.org/10.1038/s41467-022-30269-9
24. Payne LJ et al (2021) Identification and classification of antiviral defence systems in bacteria and archaea with PADLOC reveals new system types. Nucleic Acids Res 49:10868–10878.

https://doi.org/10.1093/nar/gkab883

25. Young JC et al (2012) Phage-induced expression of CRISPR-associated proteins is revealed by shotgun proteomics in Streptococcus thermophilus. PLoS ONE 7:e38077. https://doi.org/10.1371/journal.pone.0038077
26. Stokar-Avihail A et al (2023), *Discovery of phage determinants that confer sensitivity to bacterial immune systems. Cell 186, 1863–1876 e1816* https://doi.org/10.1016/j.cell.2023.02.029
27. Niault T, van Houte S, Westra E, Swarts DC (2025) Evolution and ecology of anti-defence systems in phages and plasmids. Curr Biol 35:R32–R44. https://doi.org/10.1016/j.cub.2024.11.033
28. Monk IR, Shah IM, Xu M, Tan MW, Foster TJ (2012) Transforming the untransformable: application of direct transformation to manipulate genetically Staphylococcus aureus and Staphylococcus epidermidis. *mBio* 3. https://doi.org/10.1128/mBio.00277-11
29. Corvaglia AR et al (2010) A type III-like restriction endonuclease functions as a major barrier to horizontal gene transfer in clinical Staphylococcus aureus strains. Proc Natl Acad Sci U S A 107:11954–11958. https://doi.org/10.1073/pnas.1000489107
30. Moller AG, Petit RA 3rd, Read TD (2022) Species-Scale Genomic Analysis of Staphylococcus aureus Genes Influencing Phage Host Range and Their Relationships to Virulence and Antibiotic Resistance Genes. *mSystems* 7, e0108321 https://doi.org/10.1128/msystems.01083-21
31. Rousset F et al (2022), *Phages and their satellites encode hotspots of antiviral systems. Cell Host Microbe 30, 740–753 e745* https://doi.org/10.1016/j.chom.2022.02.018
32. Beamud B, Benz F, Bikard D (2024) Going viral: The role of mobile genetic elements in bacterial immunity. Cell Host Microbe 32:804–819. https://doi.org/10.1016/j.chom.2024.05.017
33. Hossain M, Aslan B, Hatoum-Aslan A (2024) Tandem mobilization of anti-phage defenses alongside SCCmec elements in staphylococci. Nat Commun 15:8820. https://doi.org/10.1038/s41467-024-53146-z
34. Azarian T et al (2021) Genomic Epidemiology and Global Population Structure of Exfoliative Toxin A-Producing Staphylococcus aureus Strains Associated With Staphylococcal Scalded Skin Syndrome. Front Microbiol 12:663831. https://doi.org/10.3389/fmicb.2021.663831
35. Lamand V et al (2012) Epidemiological data of staphylococcal scalded skin syndrome in France from 1997 to 2007 and microbiological characteristics of Staphylococcus aureus associated strains. Clin Microbiol Infect 18:E514–521. https://doi.org/10.1111/1469-0691.12053
36. Aung MS et al (2016) Drug resistance and genetic characteristics of clinical isolates of staphylococci in Myanmar: high prevalence of PVL among methicillin-susceptible Staphylococcus aureus belonging to various sequence types. New Microbes New Infect 10:58–65. https://doi.org/10.1016/j.nmni.2015.12.007
37. Ghebremedhin B et al (2009) Emergence of a community-associated methicillin-resistant Staphylococcus aureus strain with a unique resistance profile in Southwest Nigeria. J Clin Microbiol 47:2975–2980. https://doi.org/10.1128/JCM.00648-09

38. Thuy DB et al (2021) Colonization with Staphylococcus aureus and Klebsiella pneumoniae causes infections in a Vietnamese intensive care unit. Microb Genom 7. https://doi.org/10.1099/mgen.0.000514
39. Glaser P et al (2016), *Demography and Intercontinental Spread of the USA300 Community-Acquired Methicillin-Resistant Staphylococcus aureus Lineage. mBio 7, e02183-02115* https://doi.org/10.1128/mBio.02183-15
40. Alam MT et al (2015), *Transmission and microevolution of USA300 MRSA in U.S. households: evidence from whole-genome sequencing. mBio 6, e00054* https://doi.org/10.1128/mBio.00054-15
41. Depardieu F et al (2016) A Eukaryotic-like Serine/Threonine Kinase Protects Staphylococci against Phages. Cell Host Microbe 20:471–481. https://doi.org/10.1016/j.chom.2016.08.010
42. Maestri A et al (2024), *The bacterial defense system MADS interacts with CRISPR-Cas to limit phage infection and escape. Cell Host Microbe 32, 1412–1426 e1411* https://doi.org/10.1016/j.chom.2024.07.005
43. Rostol JT, Quiles-Puchalt N, Iturbe-Sanz P, Lasa I, Penades JR (2024) Bacteriophages avoid autoimmunity from cognate immune systems as an intrinsic part of their life cycles. Nat Microbiol 9:1312–1324. https://doi.org/10.1038/s41564-024-01661-6
44. Novick RP, Christie GE, Penades JR (2010) The phage-related chromosomal islands of Gram-positive bacteria. Nat Rev Microbiol 8:541–551. https://doi.org/10.1038/nrmicro2393
45. Thabet MA, Penades JR, Haag AF (2023) The ClpX protease is essential for inactivating the CI master repressor and completing prophage induction in Staphylococcus aureus. Nat Commun 14:6599. https://doi.org/10.1038/s41467-023-42413-0
46. Tormo-Mas MA et al (2010) Moonlighting bacteriophage proteins derepress staphylococcal pathogenicity islands. Nature 465:779–782. https://doi.org/10.1038/nature09065
47. Debiasi-Anders G, Qiao C, Salim A, Li N (2025) Mir-Sanchis, I. Phage parasites targeting phage homologous recombinases provide antiviral immunity. Nat Commun 16:1889. https://doi.org/10.1038/s41467-025-57156-3
48. Kreiswirth BN et al (1983) The toxic shock syndrome exotoxin structural gene is not detectably transmitted by a prophage. Nature 305:709–712. https://doi.org/10.1038/305709a0
49. Baba T et al (2002) Genome and virulence determinants of high virulence community-acquired MRSA. Lancet 359:1819–1827. https://doi.org/10.1016/s0140-6736(02)08713-5
50. Diep BA et al (2006) Complete genome sequence of USA300, an epidemic clone of community-acquired meticillin-resistant Staphylococcus aureus. Lancet 367:731–739. https://doi.org/10.1016/S0140-6736(06)68231-7
51. Prjibelski A, Antipov D, Meleshko D, Lapidus A, Korobeynikov A (2020) Using SPAdes De Novo Assembler. Curr Protoc Bioinf 70:e102. https://doi.org/10.1002/cpbi.102
52. Bouras G et al (2023) Pharokka: a fast scalable bacteriophage annotation tool. Bioinformatics 39. https://doi.org/10.1093/bioinformatics/btac776

53. Bouras G, Grigson SR, Papudeshi B, Mallawaarachchi V, Roach MJ, Dnaapler (2024) A tool to reorient circular microbial genomes. J Open Source Softw 9. https://doi.org/10.21105/joss.05968
54. Nishimura Y et al (2017) ViPTree: the viral proteomic tree server. Bioinformatics 33:2379–2380. https://doi.org/10.1093/bioinformatics/btx157
55. Letunic I, Bork P (2024) Interactive Tree of Life (iTOL) v6: recent updates to the phylogenetic tree display and annotation tool. Nucleic Acids Res 52:W78–W82. https://doi.org/10.1093/nar/gkae268
56. Shang J, Peng C, Liao H, Tang X, Sun Y (2023) PhaBOX: a web server for identifying and characterizing phage contigs in metagenomic data. Bioinform Adv 3:vbad101. https://doi.org/10.1093/bioadv/vbad101
57. Bortolaia V et al (2020) ResFinder 4.0 for predictions of phenotypes from genotypes. J Antimicrob Chemother 75:3491–3500. https://doi.org/10.1093/jac/dkaa345
58. Eddy SR, Accelerated Profile HMM, Searches (2011) PLoS Comput Biol 7:e1002195. https://doi.org/10.1371/journal.pcbi.1002195
59. Page AJ et al (2015) Roary: rapid large-scale prokaryote pan genome analysis. Bioinformatics 31:3691–3693. https://doi.org/10.1093/bioinformatics/btv421
60. Page AJ et al (2016), *SNP-sites: rapid efficient extraction of SNPs from multi-FASTA alignments. Microb Genom 2, e000056* https://doi.org/10.1099/mgen.0.000056
61. Price MN, Dehal PS, Arkin AP (2010) FastTree 2–approximately maximum-likelihood trees for large alignments. PLoS ONE 5:e9490. https://doi.org/10.1371/journal.pone.0009490
62. Jones P et al (2014) InterProScan 5: genome-scale protein function classification. Bioinformatics 30:1236–1240. https://doi.org/10.1093/bioinformatics/btu031
63. Truong-Bolduc QC et al (2015) Role of the Tet38 Efflux Pump in Staphylococcus aureus Internalization and Survival in Epithelial Cells. Infect Immun 83:4362–4372. https://doi.org/10.1128/iai.00723-15
64. Hisatsune J et al (2016) Efficient transformation of Staphylococcus aureus using multi-pulse electroporation. J Microbiol Methods 130:69–72. https://doi.org/10.1016/j.mimet.2016.08.012
65. Kato F, Sugai M (2011) A simple method of markerless gene deletion in Staphylococcus aureus. J Microbiol Methods 87:76–81. https://doi.org/10.1016/j.mimet.2011.07.010
66. Baba T et al (2002) Genome and virulence determinants of high virulence community-acquired MRSA. Lancet 359:1819–1827. https://doi.org/10.1016/s0140-6736(02)08713-5
67. Diep BA et al (2006) Complete genome sequence of USA300, an epidemic clone of community-acquired meticillin-resistant Staphylococcus aureus. Lancet 367:731–739. https://doi.org/10.1016/S0140-6736(06)68231-7

Figures

Fig. 1.

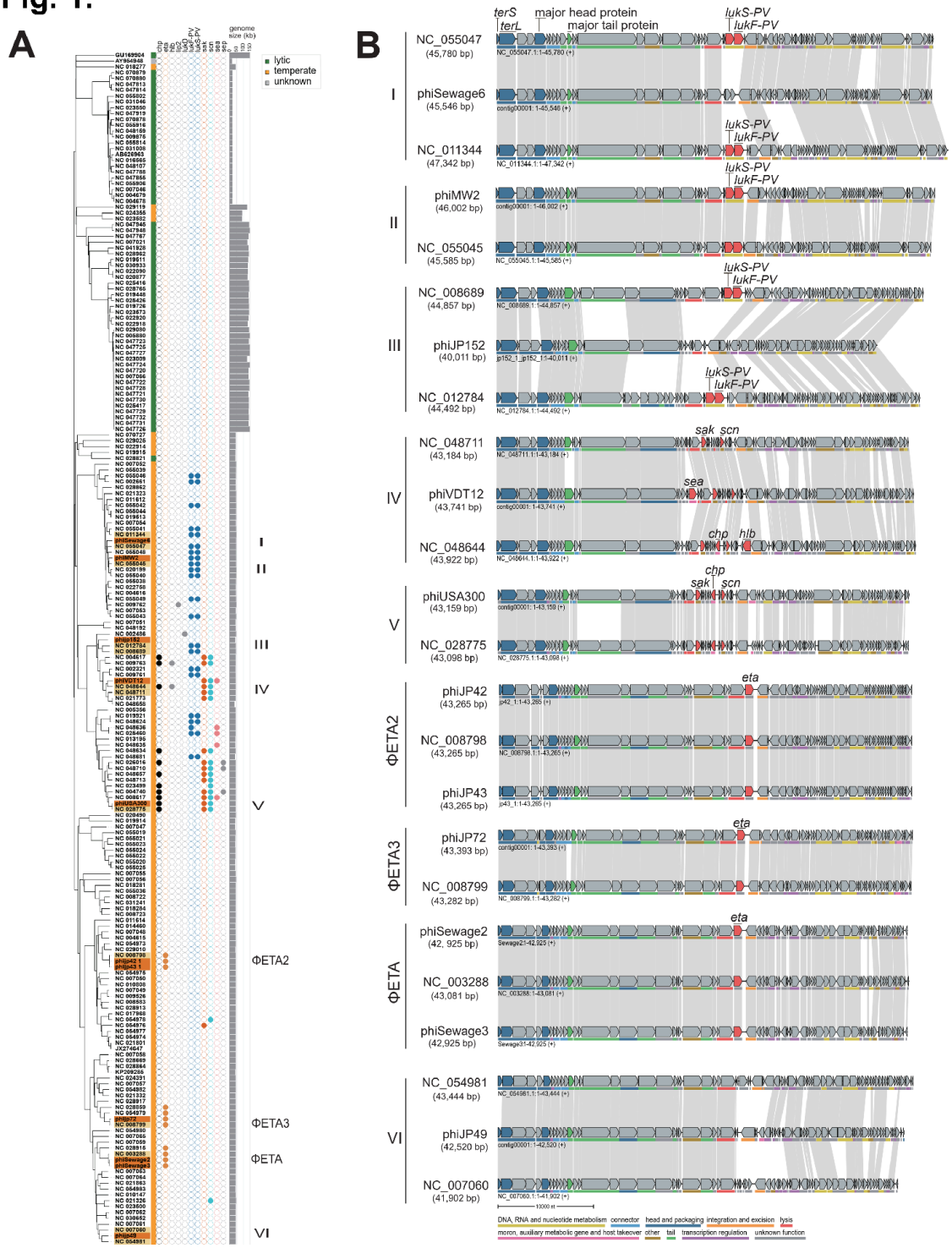


Figure 1

Phylogenetic and comparative genomic analysis of 11 *S. aureus* phages identified in this study

(A) Genome-based phylogenetic tree including 193 *Staphylococcus* phages retrieved from the ViPTree database and 11 phages isolated from *S. aureus* in this study. Phages identified in this study are shown in orange, and the closely related phages selected for comparison in panel **(B)** are shown in light orange.

Tracks to the right of the phage names indicate predicted lifestyle (lytic, temperate, or unknown), as determined using PhaBOX, the presence or absence of virulence factor genes (*chp, eta, hlb, lip2, lukD, lukS-PV, lukF-PV, sak, scn, sea,* and *sep*), and genome size. **(B)** Whole-genome comparison of the 11 phages identified in this study and their phylogenetically related reference phages highlighted in light orange in (A). Conserved structural genes, including *terS*, *terL*, and major head protein genes, are shown in blue, whereas major tail protein genes are shown in green. Virulence factor genes, including *lukF-PV*, *lukS-PV*, *eta, sak, chp, scn, hlb*, and *sea*, are indicated by red arrows.

Fig. 2.

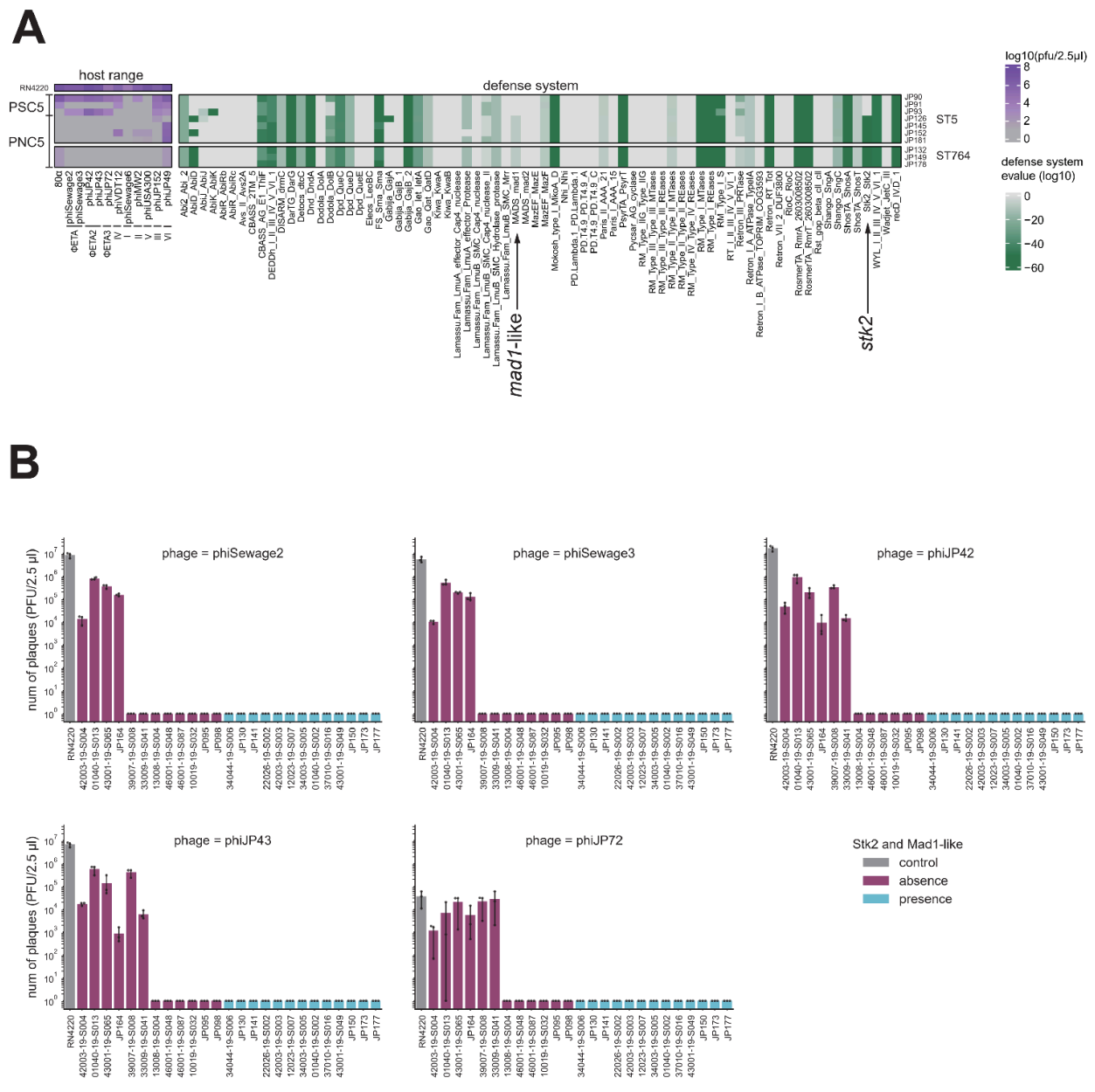


Figure 2

Association between phage defense systems and phage susceptibility in CC5 strains

(A) Heatmap of phage host range across 10 CC5 (ST5/ST764) strains. Strains are grouped as phage-susceptible CC5 (PSC5) and phage-non-susceptible CC5 (PNC5), as indicated in the figure. Phage infectivity was evaluated using representative temperate phages and is expressed as $\log_{10}$ PFU/2.5 µL. Defense systems detected in each strain are shown in the right-hand heatmap as DefenseFinder E-values. Black arrows indicate two predicted phage defense systems: *stk2* and a *mad1*-like defense system. **(B)** Spot assay of an expanded panel of CC5 strains examining the relationship between *stk2* and *mad1*-like systems and susceptibility to the same representative *eta*-carrying temperate phages as in Fig. 2A. A total of 25 CC5 strains were tested: 12 lacking both *stk2* and *mad1*-like (cyan), and 13 carrying both systems (light blue). For each phage, strain names are shown on the x-axis and phage infectivity on the y-axis as plaque count (PFU/2.5 µL).

Fig. 3.

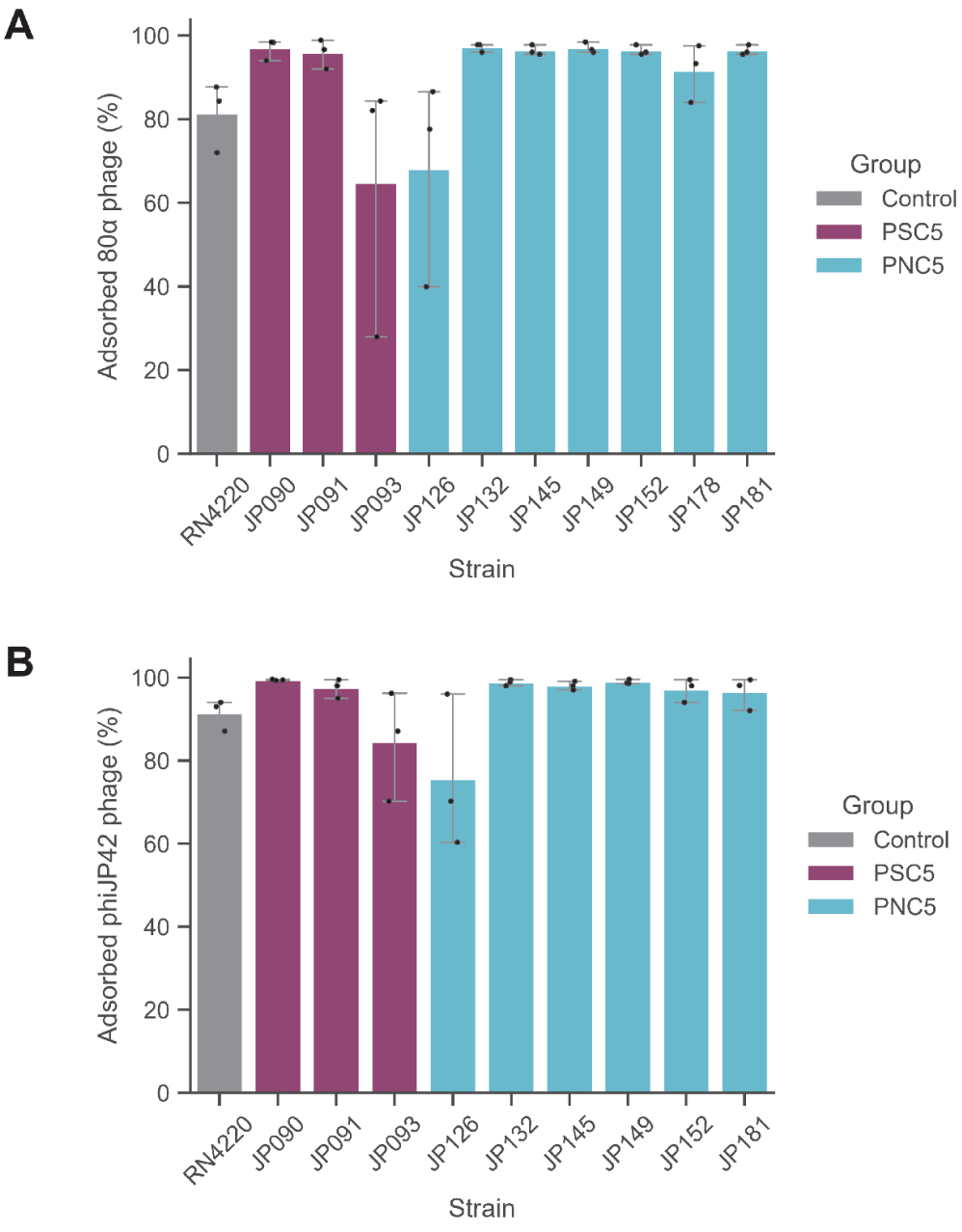


Figure 3

Phage adsorption efficiency in the CC5 lineage

Adsorption of **(A)** phage 80α (MOI = 0.1) and **(B)**phiJP42 (MOI = 0.01) was measured using RN4220 and clinical CC5 isolates, as described in the Methods. Adsorption was measured 10 min after phage addition, and the y-axis shows adsorption efficiency (%). Bars and error bars indicate the mean ± SD of

three independent experiments (n = 3), and each point represents an independent experiment. Kruskal–Wallis test: **(A)** *P* = 0.0229; **(B)** *P*= 0.0325.

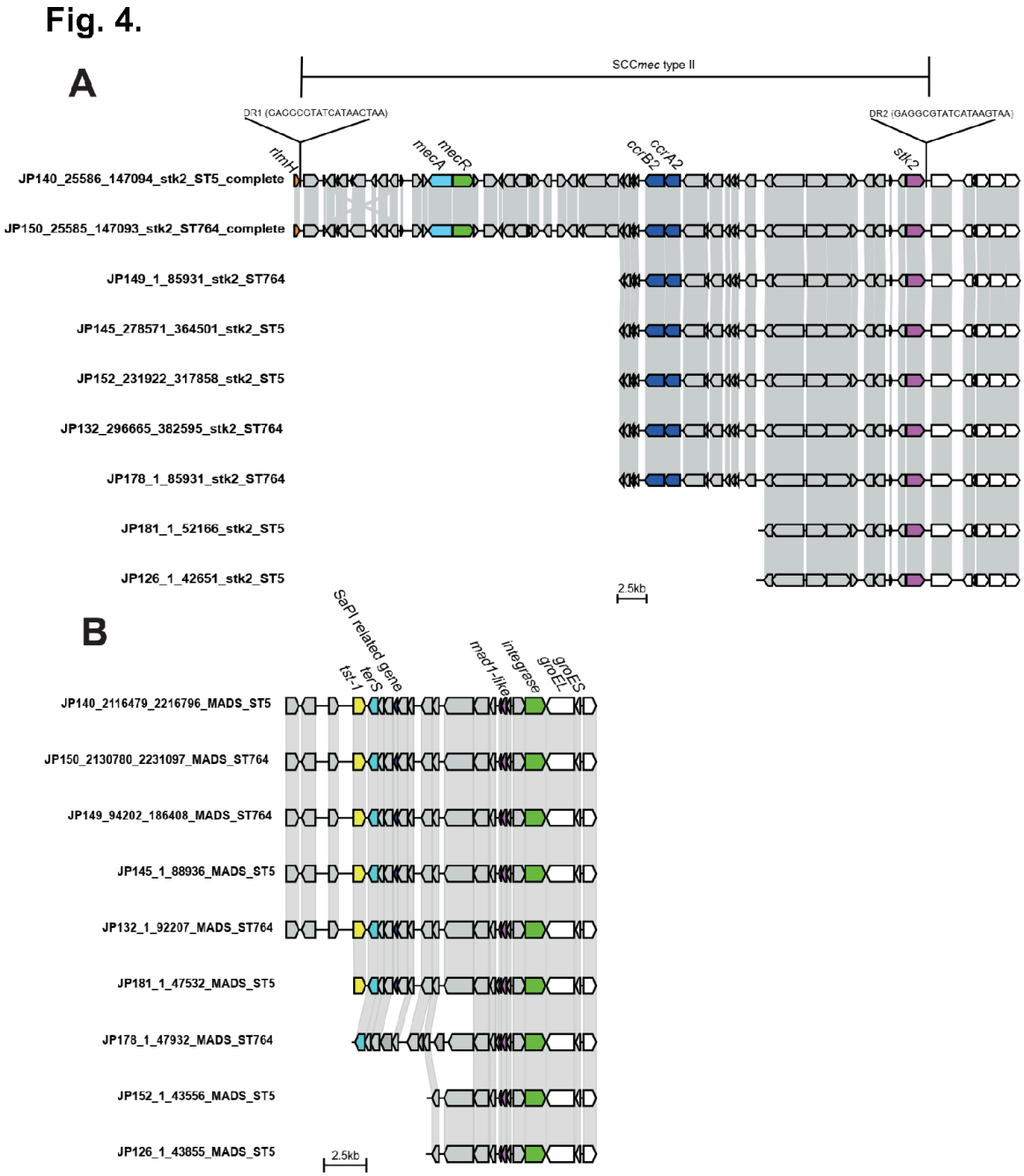


Figure 4

Genomic locus comparison of *mad1*-like and *stk2* loci

Seven CC5 strains used in the host-range assay, together with two strains with complete reference genomes, JP150 (ST764) and JP140 (ST5), were included in the analysis. Genomic regions flanking each phage defense system were extracted and visualized using clinker v0.0.28. Links between homologous genes are shaded according to amino acid sequence identity and do not reflect similarities in intergenic regions. In the *stk2* locus **(A)**, representative genes are color-coded as follows: *ccrAB*, blue; *mecA*, sky blue; *mecR*, green; *stk2*, purple; and *rlmH*, orange. In the *mad1*-like locus **(B)**, *tst-1* is shown in yellow, *terS* in blue, integrase in green, and *mad1*-like in purple.

Fig. 5.

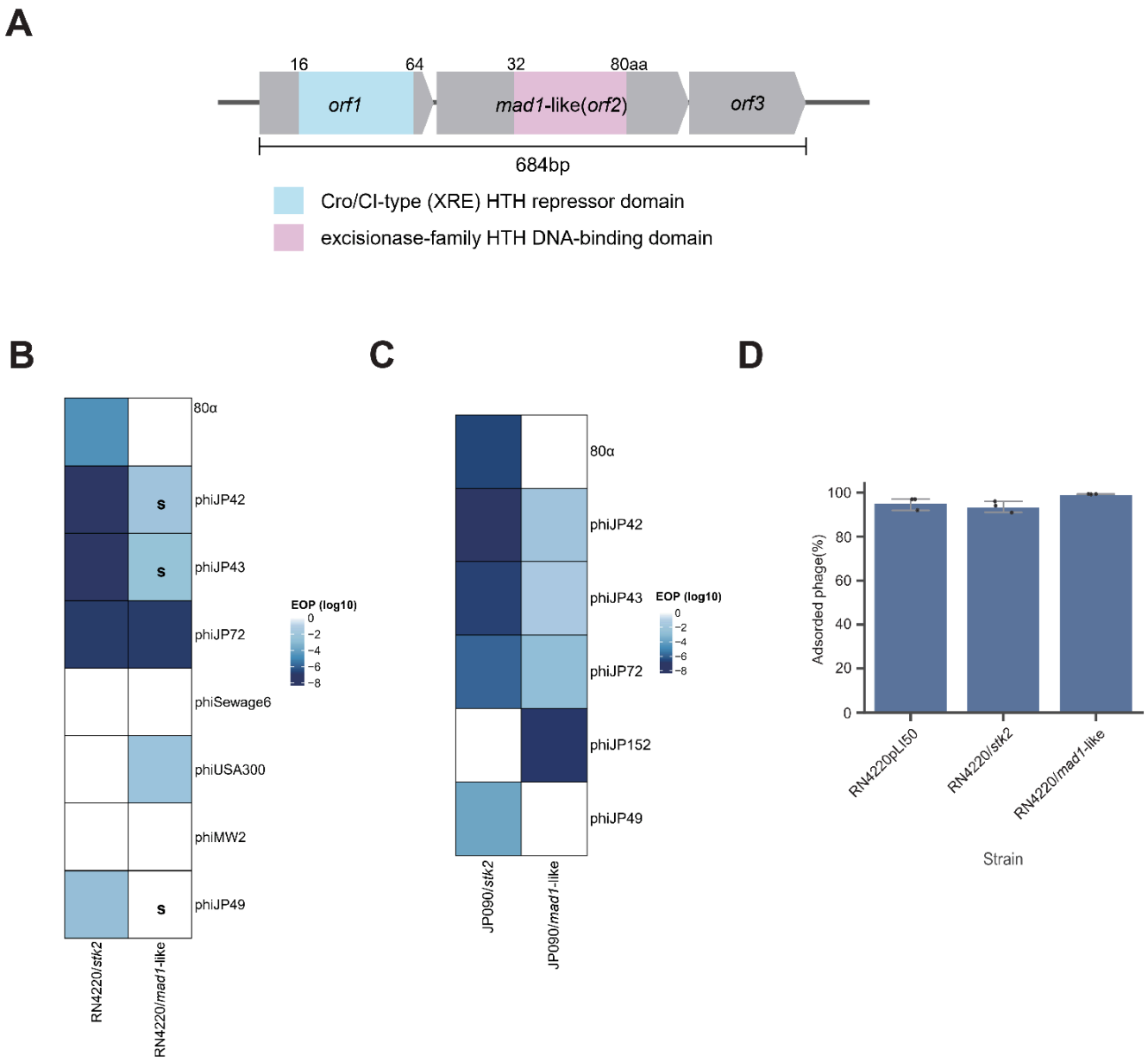


Figure 5

Antiphage defense activities of *stk2* and the *mad1-like*operon in CC5 strains

(A) Schematic of the *mad1*-like system, organized as a three-gene operon (*orf1–orf3*). Domain assignments are detailed in Supplementary Table 7. **(B)** Phage susceptibility spot assays using *S. aureus* RN4220 carrying pLI50 expressing *stk2* or the *mad1*-like operon, with RN4220 carrying the empty pLI50 vector as a control. Strains were challenged with the phages indicated in the panel. Defense activity is expressed as the log efficiency of plating (EOP) relative to the empty vector control; blue indicates reduced EOP and white indicates EOP ≥ 1. “S” denotes reduced plaque size in addition to inhibited infection. Assays were performed in three independent biological replicates (n = 3). **(C)** Phage susceptibility spot assays using JP090-derived transformants carrying the empty pLI50 vector, pLI50/*stk2*, or pLI50/*mad1*-like, performed as described in (B). Phage titers (PFU/mL) for Fig. (B) and (C) are listed in Supplementary Table 8. In (B) and (C), phages yielding plaques too small for reliable counting on TSA-CP10 in either the reference or test host were excluded from the analysis and are not shown. (**D**) Adsorption of phage phiJP42 to plasmid-transformed RN4220 strains carrying the empty pLI50 vector, pLI50/*stk2*, or pLI50/*mad1*-like was measured 10 min after phage addition (MOI = 0.1). The y-axis shows adsorption efficiency (%). Bars and error bars represent mean ± SD of three independent experiments (n = 3); each point corresponds to an individual experiment. Overall group comparison: Kruskal–Wallis test (P = 0.0496); pairwise Mann–Whitney U tests with Holm correction revealed no significant differences between individual groups.

Supplementary Files

This is a list of supplementary files associated with this preprint. Click to download.

- Supplementarytable.xlsx
- SuppFig.pdf